Contrib Mineral Petrol (1994) 115:402–414

Contributions to Mineralogy and Petrology

Effects of magma storage and ascent on the kinetics of crystal growth

The case of the 1991–93 Mt. Etna eruption

P. Armienti[1], M.T. Pareschi[1], F. Innocenti[2], and M. Pompilio[3]

[1] Dipartimento di Scienze della Terra, via S. Maria 53, I-56126 Pisa, Italy
[2] CSGSDA-C.N.R., via S. Maria 53, I-56126 Pisa, Italy
[3] IIV-C.N.R., piazza Roma 2, I-95123 Catania, Italy

Received November 26, 1992/Accepted August 2, 1993

Abstract. The size distributions of crystals of olivine, plagioclase and oxides of the 1991/93 eruption at Mt. Etna (Italy) are analyzed. The simultaneous collection of this information for different minerals gives precious insight into the cooling history of lavas. Three distinct episodes are detectable: a storage of the magma in a deep reservoir, characterized by nearly constant and low nucleation and growth rates (near to equilibrium); an ascent phase, with an ever increasing nucleation rate related to volatile exsolution; and finally a quenching phase. In addition to geochemical and geophysical evidence, the similarity of the crystal size distributions of the present eruption with those of previous ones of this century makes it possible to exclude that crystal size distributions of Etnean lavas are due to mixing of different populations. This strongly suggests that the main features of the volcano feeding system have not changed despite observed variations in the magma output rates.

Introduction

The cooling history of lavas is related to crystal population since both nucleation and growth processes are strongly dependent on the degree of undercooling (Kirkpatrick 1977; Dowty 1980). Indeed, if the crystals observed are those which nucleated and grew in the magma, without any loss or gain of grains, their number AND size are dependent on the kinetic constants of their nucleation and growth equations (Cashman 1990). Thus, temporal information can be extracted from lava modes if we know how crystals nucleate and grow during transport and cooling processes. As pointed out by Marsh (1988) and Cashman and Marsh (1988), rock modes are better interpreted if they are represented as a crystal size distribution (CSD). The poor knowledge of the laws of nucleation and crystal growth in natural silicatic melts hampers a direct utilization of CSD to determine the time frame for rock formation (Brandeis and Jaupart 1987; Spohn et al. 1988). However natural systems are often saturated by several phases having the same cooling history. Thus, information on magma transport and cooling processes can be increased by the simultaneous collection of CSDs in the multiphase assemblage.

Mt. Etna represents a laboratory for reconstructing magma cooling processes using lava CSDs, due to the eruption frequency and the availability of temporally ordered samples. Moreover, available geophysical and petrologic knowledge allows the behaviours deduced from CSDs to be inserted in a more complete framework. We collected modal data on specimens taken directly from the surface of the lava flow during the first six months of 1991–93 eruption. In particular we attempted to recognize in the CSDs the main steps of Mt. Etna's polybaric crystallization history as documented in the more recent cycle of activity. The effects of cooling during the flow on the crystal population were evaluated by taking samples both at the eruptive vents and at the fronts. Sampling procedures were also evaluated by determining CSDs of specimens quenched in water and cooled in air.

Volcanologic and petrographic outlines

On the morning of December 14, 1991, a seismic swarm accompanied the opening and propagation of a fissure radiating SSE from the summit of Mt. Etna (Barberi et al. 1992). Near to the Southeast Crater the fracture gave rise to a short episode of lava fountains and to a small lava flow which lasted a few hours. The eruptive activity resumed that night lower in the fracture, on the western wall of Valle del Bove, with a quiet effusion of degassed lavas from vents at about 2200 m a.s.l. and weak strombolian activity from 2200 to 2400 m a.s.l. In this period a varying output rate, in the range of a few tens of cubic metres per second, was observed. The eruption died by the end of March 1993 having reached a volume of at least 300×10^6 m^3, the largest in the last three centuries (Barberi et al. 1992). Several temperature measurements in the 1060–1080°C range were carried out at ephemeral vents, at depths varying from 10 to 40 cm in the flow. Both composition and output rate varied during the first week of the eruption until conditions steadied in the feeding

Correspondence to: P. Armienti

Table 1. Mean chemical and modal composition of Mt. Etna lavas of the eruptions of 1991/93 (period Dec/15/91–May/28/92) and 1989 (lavas from the SE Crater). Analytical precision for XRF determination of K_2O and Rb is respectively $\pm 0.72\%$ and 2.9% (1σ)

	1991–92		1989 (CSE)	
	wt.% (N=47)	SD $\pm 1\sigma$	wt.% (N=16)	SD $\pm 1\sigma$
SiO_2	47.96	0.32	47.59	0.37
TiO_2	1.70	0.05	1.77	0.06
Al_2O_3	18.05	0.26	17.79	0.35
Fe_2O_3	3.41	0.44	3.47	0.60
FeO	6.70	0.51	6.97	0.50
MnO	0.18	0.01	0.18	0.01
MgO	5.47	0.13	5.41	0.24
CaO	9.98	0.18	10.37	0.21
Na_2O	3.81	0.09	3.54	0.08
K_2O	1.82	0.04	1.94	0.06
P_2O_5	0.46	0.02	0.44	0.02
LOI	0.45	0.08	0.54	0.08
D.I.	38.2		36.6	
Rb (ppm)	42	1.66	46.8	1.47
Mean modal composition				
	Vol% (N=8)	SD $\pm 1\sigma$	Vol% (N=5)	SD $\pm 1\sigma$
Plg	19.3	1.2	22	3.1
Ol	2.3	1.2	2	0.6
Cpx	8.5	1.6	8.4	1.3
Ti–Mt	1.2	0.2	0.6	0.3
P.I.	31.2	1.6	32.9	2.9

conduit. This study used only samples emitted after uniformity of chemical and mineralogic composition were reached and covers the period December 91–July 92. Beyond this date a change in emission rate and in the Sr isotope compositions suggest the arrival of another batch of magma. Detailed petrographic and geochemical data for about 60 samples collected during the first year of the eruption are given in Armienti et al. (1993).

Like other products of Mt. Etna in the last two hundred years, these lavas are mildly alkaline porphyritic hawaiites, with phenocrysts of plagioclase, augite and olivine (approximately in the ratio 1:1/2:1/8) joined by magnetite in the groundmass. Crystals have euhedral habits, and skeletal forms only occur in the groundmass; rare anhedral crystals of olivine and plagioclase with rounded habits are interpreted as xenocrysts. Clinopyroxenes occur more often as glomerophyric aggregates than as isolated crystals. Table 1 reports the mean modal composition of the lavas: the porphyritic index is around 30. Minerals are zoned: olivine compositions cover the range Fo 82–68, but most are near Fo 72–74 range. Both plagioclase and augite often display oscillatory zoning, and the largest plagioclase crystals have two distinct fringes with abundant glass inclusions, probably linked to faster growth. The composition of plagioclase is in the An 87–42 range, that of augite varies between Wo 50–43, En 43–33, Fs 17–10. Oxides are Ti-magnetite in the Usp 27–42 range. Samples quenched in water display abundant light brown glass with sparse crystallites of plagioclase and clinopyroxene; samples cooled in air have a black mesostasis with intersertal glass in which abundant skeletal crystals of magnetite join dominant plagioclase and augite. Vesicles vary in abundance, but the majority of samples are scoriaceous.

Mt. Etna hawaiites show compositional and mineralogic evidence of a polybaric crystallization history (Armienti et al. 1988) on a multiply saturated cotectic Ol + Cpx + Plg; the *P–T* crystallization range was estimated for 1983 lavas that are mineralogically and geochemically similar to those examined in this study. According to Trigila et al. (1990) phenocrysts in 1983 lavas crystallized under water rich conditions (1.0–2.3 wt.% H_2O) in a *T–P* range of 1096–1112°C and 85–255 MPa, corresponding to crustal depths of 3–10 km. The cotectic nature of the liquid line of evolution is confirmed by thermodynamic calculations (Ghiorso et al. 1983) performed at oxygen fugacity 1 log unit above QFM, at varying pressure and water contents. Our computations show that the low pressure (0.1–200 MPa) liquidus phase of Mt Etna hawaiites is invariably olivine followed within 20°C by plagioclase and clinopyroxene; higher pressure (400 MPa) stabilizes calcic clinopyroxene as the liquidus phase, rapidly joined by olivine and plagioclase. In all the tests, Ti-magnetite always appears last on the liquidus. The very rare Fo-rich olivine found in 1991–93 lavas are considered to be relicts of a more primitive stage, while those in the range Fo 75 (cores of phenocrysts) Fo 72 (rims of phenocrysts and groundmass) are equilibrium phases of hawaiite and its residual liquids. High H_2O contents characterize Mt Etna lavas, as it is shown by fluid inclusion and mineralogic studies (Metrich et al. 1993; Sobolev et al. 1990; Dolfi and Trigila 1983). Thus, the labradoritic composition of some plagioclase nuclei and of crystals enclosed in olivine phenocrysts, points to an early cotectic crystallization of this phase on the hawaiitic liquidus, under high partial pressure of water.

Geochemical evidence suggests that Mt. Etna is fed by distinct magma pulses that reach the surface bearing a compositional imprint of their independent origin. The absence of large-scale mixing events at depth is demonstrated by the last two eruptions: the mean composition of the 1989 lavas of the SE Crater is reported in Table 1. It is evident that their slightly less evolved composition, with respect to the lavas of 1991–93, couples with higher contents of incompatible elements like K_2O and Rb. No obvious fractionation mechanism relates the two compositions and we must conclude that the 1991–93 eruption was fed by a distinct magma pulse. This same situation occurred in the consecutive eruptions of 1971 (DI = 37, K_2O = 1.66%, Rb 37 ppm) and 1974 (DI = 35, K_2O = 1.91, Rb = 44 ppm). In addition, differences in Sr isotopic composition of lavas emitted in the last twenty years (Armienti et al. 1989) rules out the possibility of a large storage system during this period, within which mixing and homogenization of magmas can take place.

Methods

Modal data are reported as CSDs, i.e. the number $n(L)$ of crystals per unit volume and unit size, as a function of their linear dimension L (Marsh 1988; Cashman and Marsh 1988; Maaløe et al. 1989). CSDs were collected on digitized images of thin sections in which grains of interest (plagioclase, olivine, clinopyroxene, oxides and vesicles) are separated from the background by segmentation techniques (Allard and Sotin 1988). Binary images of plagioclase and opaques were obtained with image acquisition system and VISILOG software, mounted on a PC connected to a microscope for optical mineralogy. Binary images of olivine, clinopyroxene, plagioclase and opaques were also obtained combining digitized X-ray maps of elements, taken with an EDS microanalyser (LINK ExL equipped with FEATURE SCAN) linked to a Cambridge Stereoscan360 SEM. This last procedure, although time consuming, tested the reproducibility of the optical methods and allowed us to determine the size distribution of phases such as olivine and clinopyroxene which, in our case, are not easily distinguishable using optic images. Controls guaranteed the perfect overlap of CSDs detected with the two methods (see, e.g. Fig. 1 for plagioclase crystals). Sample labels indicate day, month and year of sampling.

Grain characteristics in the plain (number, area, equivalent radius, elongation) and the reconstruction of crystal size distributions in the space, were computed by an "unfolding" technique (Pareschi et al. 1990) which derives crystal size distribution in the volume

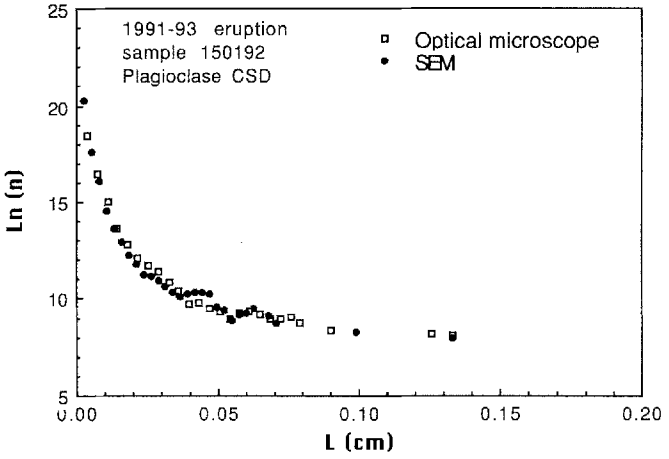

Fig. 1. Comparison between CSD acquired with optical and EDS/SEM methods in the lava sample 150192 of 1991–93 eruption of Mt. Etna

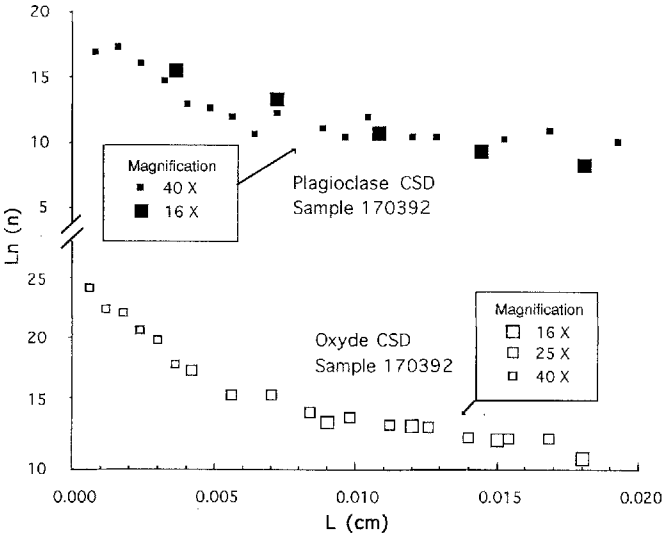

Fig. 2. Effects of increasing magnification on CSD of plagioclase and oxides. Note the stability of the number of crystals at varying magnifications and at different widths of class-size. Low magnification implies a loss of information on the smallest classes. At 16 ×, 25 × and 40 × class interval is 0.0036 cm, 0.0014 cm and 0.0008 cm respectively

from information gathered on digitized images of a thin section. The unfolding technique assumes that crystals are spherical particles with diameter L. The input datum is the distribution of crystals $n_A(L_A)$ in thin section as a function of the apparent equivalent diameter L_A (= diameter of the circle having the sectioned area of the grain). The algorithm (see Appendix I) gives acceptable results both for spherical and ellipsoidal particles with axes kL, L, L. Olivine crystals can safely be approximated as spherical particles ($k = 1$), clinopyroxene crystals and plagioclases elongated on [100] approach the situation in which one axis is larger than the other two ($k > 1$), the condition of tabular plagioclase flattened on (100) is described assuming $k < 1$. In these last two cases the reported linear dimension is approximately the minor axis as discussed in Appendix I.

The largest crystals seem to populate the largest classes in a discontinuous way (see Figs. 3–6). Indeed there is a relation between the value of $Ln(n)$ and the investigation area needed to acquire continuous CSDs (see Appendix II). The typical dimension of phenocrysts in Etnean lavas is millimetric and their abundance gives $Ln(n) \leq 9$–10; thus areas of at least 1–2 cm^2 must be investigated to guarantee continuous distribution around this size interval. In our approach we analyze areas of ~ 1.5 cm^2 on each thin section.

Figure 2 compares CSDs obtained for plagioclase and oxides in the size range 0–0.02 cm using different resolutions: 16 × magnification is the standard condition of acquisition, and allows detection of classes down to 0.003 cm. Higher magnification allows access to smaller classes, and the satisfactory overlap of the common domains (see Fig. 2) guarantees that the acquisition does not introduce bias.

Crystal balance equations

The number of crystals and the dimension they can reach depend on the cooling history; magmas are in fact populated by a number of crystals whose size changes according to the time of appearance (Dowty 1980). Peaks in the size distribution indicate a burst in the nucleation (expected for high undercooling ΔT), while flat distributions (about the same number of crystals of each size) suggest nucleation occurring at constant undercooling (Kirkpatrick 1977; Dowty 1980; Armienti et al. 1991). This behaviour can be explained on the basis of the balance equation (Marsh 1988) for the number n of crystals per unit size per unit volume:

$$\frac{\partial Vn}{\partial t} + \frac{\partial GVn}{\partial L} = Q_{in}\, n_{in} - Q_{out}\, n_{out} \tag{1}$$

where t is time, L is crystal size, V is the volume of the magma, G is the crystal growth rate and $Q_{in}n_{in}$ and $Q_{out}n_{out}$ are, respectively, the crystal influx and outflux from the system.

Consider a rising batch of magma of volume V, with no migration of crystals, and for which the only input of crystals to a given class is due to nucleation and growth mechanisms, Eq. (1) in the domain $t \geq t_i$ and $L \geq L_c$ (where t_i is the initial time and L_c is the critical radius of the crystal) reduces to:

$$\frac{\partial Vn}{\partial t} + G\frac{\partial Vn}{\partial L} = 0 \tag{2}$$

with the initial and boundary conditions:

$$Vn_{ti,Lc} = \begin{cases} 0 & \text{for } L > L_c \\ \dfrac{V(ti)\,J(ti)}{G(ti)} & \text{for } L = L_c \end{cases} \tag{3a}$$

and:

$$Vn_{t,Lc} = \frac{V(t)\,J(t)}{G(t)} \tag{3b}$$

where J is the nucleation rate. In Eq. (2), the growth rate G is assumed not to be dependent on crystal dimension L.

The solution of Eq. (2), obtained with conditions (3), is (Appendix III):

$$n(t,L) = \frac{J(t_L)\,V(t_L)}{G(t_L)\,V(t)} \tag{4}$$

where t_L is a time such that in the interval t–t_L the crystals, of the class around L at time t, grew from 0 to L. Equation (4) describes $n(L)$ at time t as a function of the ratio between the nucleation and growth rates at the time

of appearance of crystals of dimension L and that of a previous volume over the actual volume. The influence of $V(t_L)/V(t)$ on $n(L)$ is varying. For example, if the total crystallinity is between 20 and 30%, as in the case of Etnean lavas, the ratio $V(t_L)/V(t)$ varies between 1.25 and 1.43. (in a logarithmic scale such that adopted in the figures this involves, at worst, a correction of 0.36 for J/G). Therefore we can safely neglect the ratio $V(t_L)/V(t)$ and assume that the CSD is only influenced by the ratio J/G. Thus, the number density of crystals of size L at time t is equal to the nucleation density at time t_L when they appeared:

$$n(t,L) \approx \frac{J(t_L)}{G(t_L)} \tag{5}$$

Since variations in the growth rate affect all the crystals simultaneously, no size overlapping may occur between crystals born at different times and the size reached by crystals is only a function of the time they take to grow. In these systems the different trends shown by $n(L)$ reflect variations of nucleation density as the degree of undercooling increases during crystallization. At constant undercoolings, Eq. (5) guarantees that $n(L)$ is constant; thus we expect, in principle, a horizontal trend for CSD in these conditions (see also Dowty 1980).

As Marsh (1988) pointed out, however, under a condition of constant undercooling a magma chamber may also develop a log linear distribution of crystals. This condition is achieved when a crystallizing magma is continuously fed by a crystal-free melt, is periodically tapped by an eruption and is thoroughly homogeneized in the magma chamber. In this case the term $Q_{out}\, n_{out}$ in Eq. (1) is not zero, and $n(t,L)$ develops a log-linear trend with slope $= -1/G\tau$, where G is a constant growth rate and τ is the time in which the volume V of magma in the chamber is totally exchanged (Marsh 1988).

Crystal size distributions of 1991–93 lavas

Table 2 lists the samples that were analyzed for CSD and the method of sampling; a selection of CSDs of lavas chosen at the beginning, the middle and the end of the explored temporal interval (December 1991-May 1992), is reported in Figs. 3–6. All the distributions exhibit the same three distinct behaviours. Larger crystals are distributed along nearly horizontal trends (range A), with the frequent exception of oxides, which are rare as phenocrysts. Smaller crystals exhibit steeper distributions with respect to their dimension (range B), but the diameters at which each mineral displays a kink or any significant change in slope between range A and B do not vary with the time of emission and are different for each kind of mineral. Crystals with sizes less than 0.003 cm (range C) are affected by the method of quenching. Table 3 reports the mean slopes of the trends and the corresponding sizes. Similar trends are observed for clinopyroxene (Fig. 5) but we avoid interpreting its CSDs since this phase tends to form clots.

Comparison of CSDs of the different minerals (Figs. 3–6) reveals that the change in slope between portions A and B occurs at greater diameter (about double) for plagioclase than olivine. Within range B plagioclase CSDs show an increasing slope with decreasing size. Plagioclase, clinopyroxene and oxide from samples quenched in water may develop a CSD maximum for sizes less than 0.003 cm.

Qualitative information on the thermal regime prevalent during the crystallization processes may be derived by the examination of crystal habits. The experimental observations of Lofgren (1974) reveal that plagioclase develops different habits at different undercoolings. In particular low undercooling ($< 30°C$) favours the occurrence

Table 2. List of analyzed CSDs

Sample dd/mm/yy	CSD				Cooling	Locality of sampling
	Pl	Cpx	Ol	Ox		
141291L	x #	#	#	x #	air	Lava flow from SE Crater, at rest
181291	x				snow	Valle del Bove moving front
241291	x				snow	Val Calanna moving front
311291	x				snow	Val Calanna moving front
030192	x #	x #	#	x #	air	Valle del Bove, overflow near the vents
120192	x				water	Val Calanna, ephemeral vent
150192	x #	#	#	x #	water	Valle del Bove, overflow near the vents
220192b	x			x #	water	Valle del Bove, ephemeral vent next to the eruptive fracture
130292	#	#	#		water	Poggio Canfareddi, ephemeral Vent
140392b	x #				air	Val Calanna moving front
140392q	x		#		snow	Val Calanna moving front
170392	x		#	x #	water	Val Calanna moving front
220492	x				air	Overflow next to the main vent
010592	x				air	Valle del Bove, ephemeral vent
230592f	x #	#	#	x #	water	Main vent (2000 m a.s.l.)
230592v	x #	#	#	x #	water	Val Calanna, ephemeral vent (~6 km downstream)

In the first column, labels indicate the date of sampling (day, month, year). All the samples were directly taken from the lava flow while still yellow hot. The rate of cooling cannot be quantified, but increases from samples quenched in air, in snow and in water. x = determined by optical microscope images; # = determined by SEM images

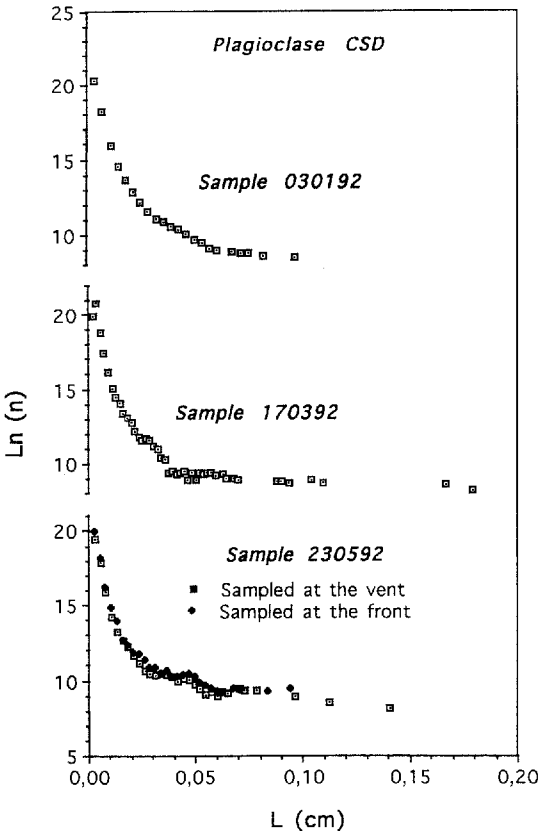

Fig. 3. CSDs of plagioclase in three lava samples for January, March and May, 1992 respectively. Sample 170392 displays a decrease of the number of crystals of the smallest size. For the sample of May, two data sets are reported: one for a sample collected at the vent and the other at the lava front, 6 km downhill. Range A ($L > 0.05$ cm) is referred to a period of deep seated growth at low undercooling; range B ($0.003 < L < 0.05$ cm) is related to the ascent of magma at increasing undercooling; Range C ($L < 0.003$ cm) is the only one generated after the emission of lavas. Some rare crystals larger than the upper limit of the scale have been also found. They have not been represented since their number density is too low respect to the investigated area to be statistically significant (see Appendix II). Data were collected at 16 × magnification

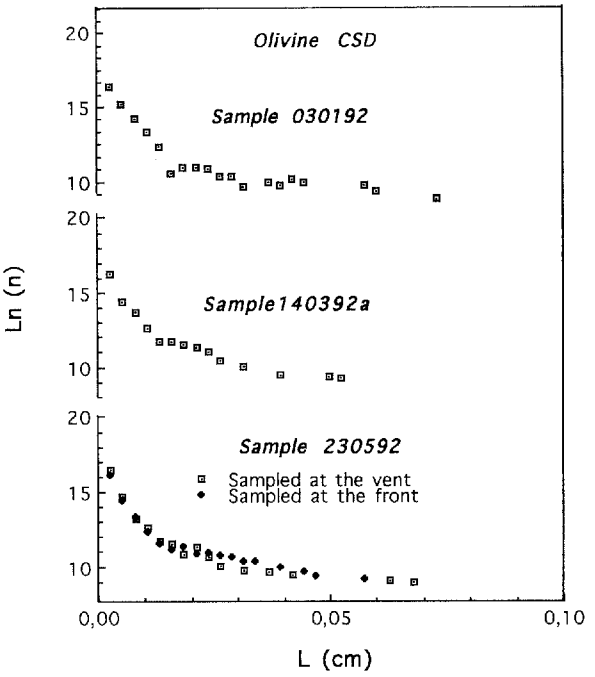

Fig. 4. CSDs of olivine in three lava samples for January, March and May, 1992. Also in this case there is a range A ($L > 0.03$ cm) with a nearly constant $n(L)$ and a range B ($0.003 < L < 0.03$ cm) where $n(L)$ sensibly increases as L decreases. The two data sets for May refer respectively to a sample collected at the vent and at the lava front. Data were collected at 16 × magnification

of tabular crystals; higher undercooling causes an increase in the elongation of crystal which start to develop acicular and finally skeletal habits. We observed that plagioclase crystals with sizes larger than about 0.015 cm are always tabular. In this interval their mean elongation ratio between the major axes in exposed sections correlates inversely with size and varies from a mean of 1.8 for crystals over 0.05 cm to 2.2 for those between 0.05–0.015 cm. Crystals smaller than 0.015 cm develop acicular shapes with an even larger elongation. These observations strongly suggest that crystallization of the studied lavas took place at increasing undercoolings, with mild undercooling reflected by the largest crystals and stronger undercooling driving growth of the smallest.

Reading crystal size distributions

Classic interpretations of porphyritic volcanic rocks identify a population of intratelluric crystals reaching

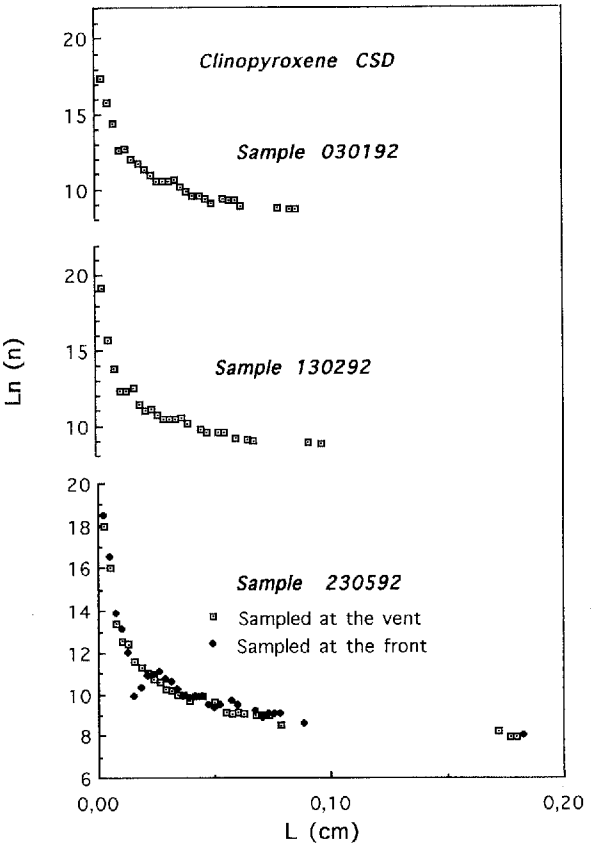

Fig. 5. CSDs of clinopyroxene in three lava samples for January, February and May, 1992. The two data sets for May refer respectively to a sample collected at the vent and at lava front. Data were collected at 16 × magnification

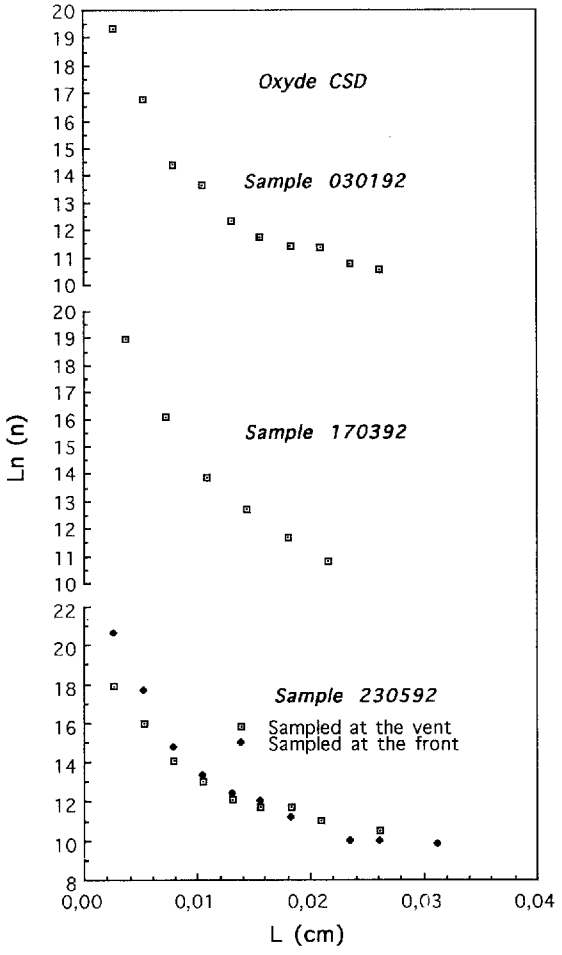

Fig. 6. CSDs of oxides in three lava samples for January, March and May, 1992. The two data sets for May refer respectively to a sample collected at the vent and at the lava front. Note the absence of nearly horizontal range which is interpreted as an evidence of the absence of Ti-magnetite as liquidus-phase in the deep seated magma (see text). Data were collected at 16 × magnification

larger size in deep seated conditions, and a population of microphenocrysts and microlites forming when lavas rise and cool rapidly upon eruption (Cox et al. 1979). In the hypothesis that no crystal is subtracted from a magmatic body or added by crystal migration mechanisms, Eq. (5) directly yields $n(L)$ as a function of the ratio J/G at the time when crystals of size L were formed.

At Mt. Etna some lavas of eccentric eruptions (e.g. 1974) reached the surface directly from the deepest part of the system (Armienti et al. 1989) and are poorly evolved, sub-aphyric basalts. In contrast lavas of the summit activity in the past 200 years are porphyritic hawaiites with variable degrees of evolution and an appreciable crystallinity (mean about 25%). Isotopic and geochemical data (Armienti et al. 1989) on several eruptions demonstrate that large-scale magma mixing has not occurred and that each eruption practically represents a single magma batch. Studies on deep (> 10 km) and shallower seismic events show seismicity distributed in a large volume beneath the volcano, thus suggesting localized stress acting near confined magma pockets (Hirn et al. 1991). Ground deformation pattern and resolution of focal mechanisms, in the case of 1989 eruptive crisis (Ferrucci et al. 1993) indicate hydraulic fracturing due to sill-like intrusions. On these bases, it appears that different batches of magma evolved in small reservoirs where they also acquired their population of phenocrysts. The base of the crust and/or a discontinuity at about 14 km (Hirn et al. 1991) are likely sites where magmas could collect in a set of distinct dykes. On these bases we can safely consider CSDs of Mt. Etna lavas as a continuous record of the cooling history of single magma batches.

Range A – intratelluric crystals

The phase of deep storage is easily identified in the range A for which CSDs slopes are close to the horizontal. According to Eq. (5), observed distributions guarantee that J/G was almost constant or only slightly varying, as expected for a system resting in a deep reservoir near thermal equilibrium. The lack of range A among the oxides of most samples is an independent evidence of the absence of Ti-magnetite on the liquidus of deep-seated magmas, in agreement with the results of experimental investigations (Dolfi and Trigila 1983) and thermodynamic calculations on the stability of the phases (Ghiorso et al. 1983).

Larger crystals of olivine and plagioclase attain sizes up to 0.3 cm but ranges A of different minerals are continuously populated only for sizes less than about 0.08 cm for plagioclase and about 0.04 cm for olivine.

Table 3. Ranges of the CSDs of 1991–93 lavas of Mt. Etna

	A	B	C
Plagioclase	$Ln(n) = 9.2–18.5L$ $L > 0.05$	$Ln(n) = 18.3–217.2L$ $0.003 < L < 0.05$	$L < 0.003$
Olivine	$Ln(n) = 10.9–30.0L$ $L > 0.03$	$Ln(n) = 15.5–212.6L$ $0.003 < L < 0.03$	$L < 0.003$
Opaques		$Ln(n) = 17.2–289.9L$ $0.003 < L < 0.027$	$L < 0.003$

The first line in each field is the regression line shown in Fig. 8 for the trends recognized in each population; L (cm) is the dimension of crystals of the ranges (see discussion in the text). The explosion of nucleation rate is underscored by the sensible increment of the average slope of $Ln(n)$ between ranges A and B

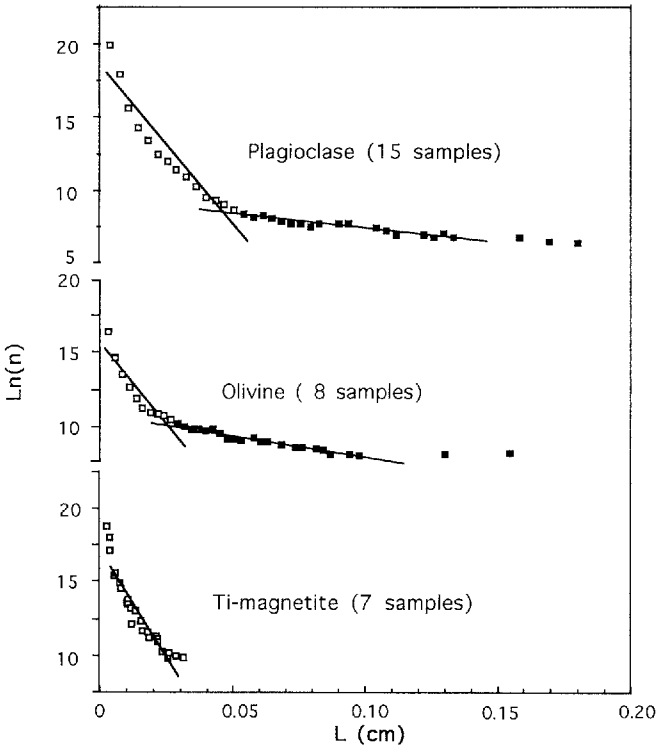

Fig. 7. Comparison between the total populations of crystals in Mt. Etna lavas of 1991–93 eruption. Shapes of distributions are the same, thus indicating the same cooling history. The limits between the ranges of each mineral are set at different values according to the dependence of respective growth and nucleation rates from the undercooling. CSDs in this figure result from the simultaneous treatment of several binary images of minerals collected on the whole data set (~ 25 cm^2 for plagioclase). This computation allows to explore the continuity of populations belonging to the largest classes (see Appendix II). Data were collected at 16 × magnification

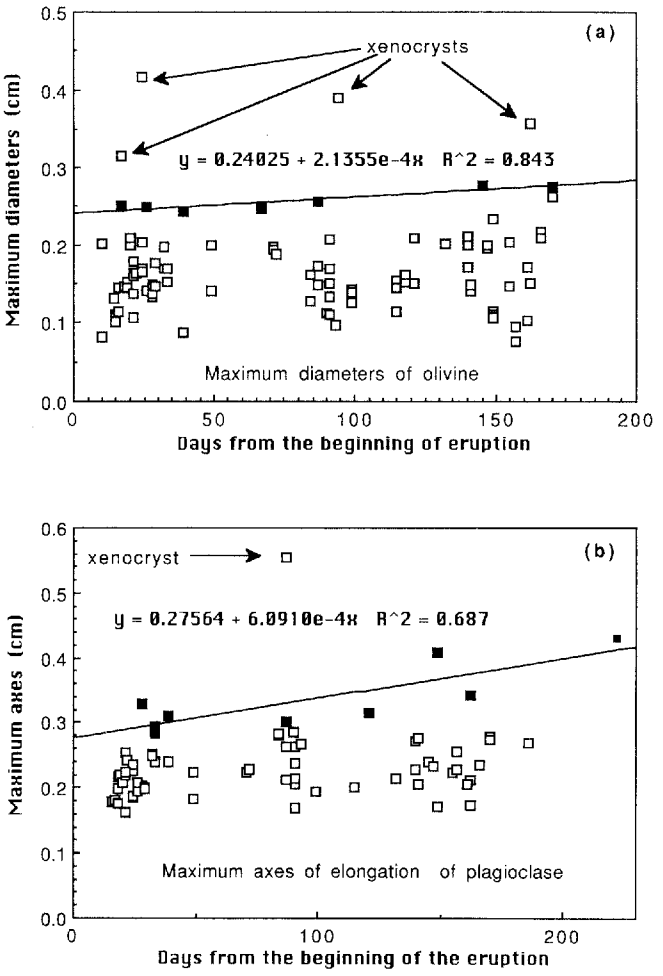

Fig. 8. a Maximum linear dimensions of olivine and **b** plagioclase crystals as a function of time from the beginning of the eruption at which the correspondent sample was collected. Each point represents a measure on a single thin section. Two thin sections of each sample were examined. When excluding xenocrysts, on the basis of their composition and habit, the upper limit of the cluster of points represents the maximum size attainable by crystals at the time of sampling. Samples for the first week are not included in the data set. In a time span of six months there is a detectable growth. The slope of the linear regression attempted on the set of black squares is an estimate (at small undercooling) of the growth rate in cm/day. R^2 is the correlation coefficient of the regression line

This implies that the distribution of larger crystals must be collected on areas larger than the 1.5 cm^2 used to determine CSDs shown in Figs. 3–6. By using the whole set of acquired binary images for plagioclase and olivine range A acquires a more continuous population (Fig. 7), confirming that large observed crystals do belong to the population developed during the storage of magma before the eruption.

Assuming that all the largest crystals formed at the same time, different sizes attained by phenocrysts might be interpreted as due to the time they spent in the deep seated reservoir. Figure 8 reports a set of measurements made on the largest olivine and plagioclase of each sample. Two sections of each specimen were examined, corresponding to about 15 cm^2 and measurements of the largest linear dimensions were done on digitized images. More sections representing several days were examined to find the largest crystals, since insufficient sections are available for a given day. In fact for $n(L) \approx e^8$ cm^{-4}, $L \approx 0.1$ cm and $\Delta l = 0.002$ cm, the area to be investigated must be greater than 5 cm^2 (see Appendix II) and becomes of the order of 100 cm^2 for a density $n(L) \approx e^5$ cm^{-4}. The maximum crystal sizes increased continuously during the five-month interval examined in this work. A maximum growth rate at depth can thus be assessed from the envelope of the maximum sizes shown in Fig. 8, under the simplified assumption of a constant growth rate.

Trends of the envelope give values of 2.4×10^{-9} cm/s for olivine and 7.1×10^{-9} cm/s for plagioclase. This estimate for olivine is similar to the one found by Armienti et al. (1991) for Lanzarote basalts at low undercooling (about one degree). The estimate of growth rate of plagioclase at low undercooling is one order of magnitude greater than those reported by Kirkpatrick (1977) for much more crystalline basalts, but compares to those found by Kirkpatrick et al. (1976) for pure anorthite and those estimated by Maaløe et. al. (1989) for basalts at undercoolings of less than one degree. The obtained value for deep plagioclase growth rate also matches those

interpreted by Cashman (1990) for the Mauna Loa 1984 eruption. The obtained values of G can be used to derive from Eq. (5) the order of magnitude of plagioclase and olivine nucleation rates at depth: assuming the values of $n(L)$ of the ranges A for olivine ($\approx 2 \times 10^4$ cm ^{4}) and plagioclase ($\approx 8 \times 10^3$ cm^{-4}), J_{ol} and J_{plag} both result in the order of 5×10^{-5} cm^{-3} s^{-1}. This plagioclase nucleation rate is two orders of magnitude below those reported by Cashman and Marsh (1988) and Kirkpatrick (1977) for Makaopuhi lava lake and approaches the values interpreted by Cashman (1988) for Mt. St. Helens dacite; values reported by Mangan (1990) for olivine nucleation rate are one order of magnitude lower than that estimated here.

The obtained growth rates allow an appraisal of the minimum times of the onset of crystallization for olivine and plagioclase. To derive this datum we have to purge measured diameters for the growth during the rise, as estimated by the kink of range A. Net deep growth is to be corrected by 0.05 cm for plagioclase and 0.03 cm for olivine. The resulting intercepts at $L = 0$ are $-980 \pm 20\%$ days for olivine and $-470 \pm 30\%$ days for plagioclase, computed with respect to the onset of eruption. The large time difference for these two minerals could be due to uncertainties in the estimates of G (ranges were extrapolated over an interval 5 times greater than the temporal interval used for their evaluation), or to slightly different temperatures (and therefore times) of first nucleation, moreover, we assumed a constant growth rate for both minerals. On July 8 and 27, 1989 (respectively 889 and 870 days before December 14, 1991 – within 10% of the estimated onset of olivine crystallization), major seismic events (M $\sim$3) accompanied an episode of magma emplacement (Ferrucci et al. 1993). These seismic events triggered a summit eruption that occurred about two months later, in September–October 1989 (Armienti at al. 1990). In any case, these earthquakes were the only major volcano-tectonic events that preceded the present major eruption (Montalto et al. 1992).

The depth of magma storage can be estimated by using measured temperatures and the P-T gradient of 10.6°C/kbar calculated by Trigila et al. (1990) in 1983 lavas for olivine-clinopyroxene equilibria: in recent Etna hawaiites the typical difference between the emission temperature ($\sim$1080°C) and the temperature of crystallization of intratelluric phases (1140–1160°C, Clocchiatti and Metrich 1984) is 60–80°C, this corresponds to a pressure drop in the range of 5.7–7.5 kbar, and suggests magma ponding at lower crust depths.

Range C – the quenching crystals

Crystals belonging to range C form after the emission of lava and their number density is strongly dependent on quenching procedure. Crystals less than 0.003 cm display acicular shapes and formed at undercoolings higher than 30°C (Lofgren 1974). Since these crystals are near the detection limit of the standard acquisition conditions, we collected a set of images on different scales for plagioclase

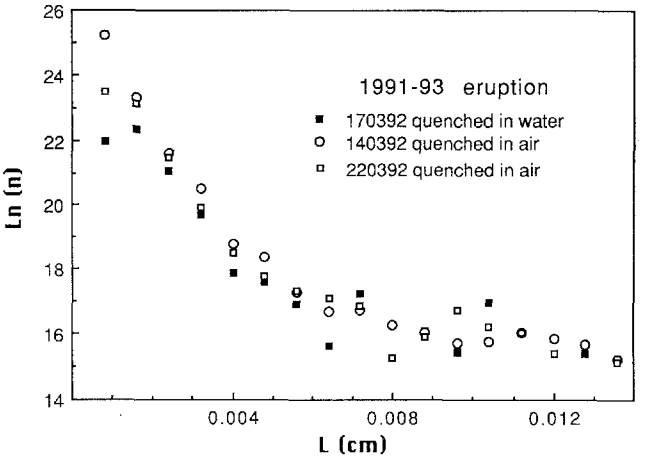

Fig. 9. CSD of plagioclase in three samples cooled at various rates. The sample quenched in water reaches the highest undercooling and displays a decrease in the number of crystals of smaller size. The two samples quenched in air reach different undercooling, as confirmed by the different number of crystals of the smallest size. These data were acquired at 25 × magnification

and oxides. Zooming the image does not alter the distributions of classes, as demonstrated by the overlapping of distributions collected with different magnifications (see Fig. 2). CSDs of samples 230592 (collected at the vent and 6 km downhill at the lava front) reveal good overlap for ranges A and B but show an increase for sizes less than 0.003 cm in the sample gathered at the front, except for olivine. The largest increment in the number of crystals is observed for Ti-magnetite, whose crystallization may be influenced by surface oxidation of lava. Oxidation process could also explain the slight downstream decrease in olivine content for sample 230592f. Figure 9 reports CSDs of plagioclase crystals collected at higher magnification in three samples cooled at various rates. Glassy groundmasses characterize samples quenched in water, while sample 140392 has a microcrystalline groundmass with scarce intersertal brown glass; in some samples quenched in water, it is possible to observe the occurrence of a maximum of CSDs in the interval C. This effect is also evident for CSDs collected at higher resolution and it is not an artefact introduced by the unfolding technique. In fact it was never observed in cases C1–C5 and E1–E6 displayed in Appendix I as a test of the unfolding technique, even when the occurrence of a detection limit was simulated by dropping in the input distribution those crystals whose cross-section on the section plane was below the assigned resolution.

Range B – crystal growth during the magma ascent

Between intratelluric phase and quenching populations, CSDs of Mt. Etna lavas reveal a set of crystals related to the cooling of magma during its ascent to the surface. Equation (5) guarantees that $n(L)$ expresses the ratio J/G and we can expect that effects due to the ascent can increase the undercooling, and therefore J/G. An accurate estimate of the total undercooling experienced by Etnean magmas during the ascent is a difficult task: many physi-

cal and composition factors may influence this value. The total temperature drop during magma rise is due to decompression, volatile exsolution (mainly CO_2 and H_2O) and heat transfer to the surroundings. It may be estimated to be on the order of 60–80°C; in fact the maximum temperature measured in lavas with a Pt-Rh thermocouple is 1080°C (Barberi et al. 1992), while homogenization of fluid inclusions in phenocrysts is typically reached in the temperature interval 1140–1160°C for Mt. Etna hawaiites (Clocchiatti and Metrich 1984). This 60–80°C interval is the maximum temperature drop of Etnean lavas during the whole crystallization interval and cannot be considered as an estimate of undercooling of lavas at the vents. Undercooling is also a function of liquidus temperature which varies during ascent due to decrease of P_{tot}, changes in composition and loss of volatiles. Examination of crystal habits allows an heuristic estimate of undercooling: plagioclase and augite crystals in the larger sizes of range B ($0.015 < L < 0.05$ cm) have, respectively, tabular and equant habits that can be interpreted, according to Lofgren (1974), as due to undercooling not greater than 30°C; the increment in plagioclase elongation for size between 0.015 and 0.003 cm indicates teven larger undercooling in the lower limit of range B. The rate at which the total (unknown) undercooling has been reached can be assessed from olivine morphology: this mineral in range B never displays the hopper forms that in dynamic crystallization experiments (Donaldson 1976) appear at cooling rates of 2.5°C/h; thus lower cooling rates are realistic during the growth of range B population.

The effect of water content on the liquidus temperature was experimentally investigated by Dolfi and Trigila (1983) for the 1971 lavas of Mt. Etna, revealing that water loss may strongly affect undercooling; similar effects were also observed by Lipman et al. (1985) in Hawaiian basalts. A further increase of undercooling at the water exsolution level may be responsible for the development of more elongated plagioclase crystals in the lower size portion of range B ($0.003 < L < 0.015$ cm) and can be related to ever increasing values of $n(L)$ particularly evident for plagioclase, clinopyroxene and Ti-magnetite. If we assume a water content of 2–2.3% for 1991–93 lavas, similar to the estimate for 1983 (Trigila et al. 1990) and older lavas (Metrich et al. 1993), we can use the equation proposed by Macpherson (1984) and the lava compositions to estimate a water exsolution level between 1.3 and 1.8 km below the summit of the volcano. This correlates with the depths of volcanic tremors of some eruptions that Scick et al. (1982) fixed at a depth of 2 km.

The positive correlation of $n(L) = J(t_L)/G(t_L)$ with undercooling can be found if the theoretical expressions for J and G found in Cashman (1990) and Toramaru (1991) are used:

$$J \propto \exp(-E/R_G T_m) \exp - \frac{16\pi\gamma^3 v_c^2 T_o^2}{3 k T_m \Delta h^2 (T_m - T_o)^2} \quad (6)$$

$$G \propto \exp(-E/R_G T_m)\left[1 - \exp\left(\frac{\Delta h\, \Delta T}{k T_o T_m}\right)\right] \quad (7)$$

where: v_c is the volume of one molecule of a crystallizing phase, R_G is the gas constant, γ is the interfacial tension between crystal and melt, T_m is magma temperature, T_o is the liquidus temperature, $\Delta T = T_m - T_o$, Δh is the enthalpy of fusion per molecule ($= k\Delta H/R_G$, where ΔH is the molar enthalpy of fusion), k is the Boltzman constant, E is the activation energy per mol. Figure 10 shows J/G (normalized to one) as a function of ΔT, for $E = 200$ kJ/mol, $\Delta H = 60$ kJ/mol, and different values of the most sensitive parameter γ (0.02, 0.1 and 0.05 J/m^2). In the graphs of Fig. 10 $T_o = 1500$ K and $v_c = 5.2 \cdot 10^{-29}$ m^3. In general, values of γ are in the range ~ 0.1 J/m^2 for olivine basaltic melt (Cooper and Kohlstedt 1982) to 0.022 J/m^2 (postulated by Dowty 1980); E is found by Hofmann (1980) in the range 60–250 kJ/mol (for alkali feldspars in a silicate melt), and typical values of ΔH are found in the order of 100 kJ/mol by Weill et al. (1980), while Toramaru (1991) used value in the range 50–80 kJ/mol. From Fig. 10 it appears that as ΔT increases, J/G always increases (cases 2 and 3), in agreement with our CSDs which show greater values of $n(L)$ for smaller crystals forming at higher undercoolings. In case 1 a maximum of J/G is found, if in Eq. (6) the interfacial tension γ is reduced to $\sim 10^{-2}$ J/m^2, a condition reached if heterogeneous nucleation becomes very important (Toramaru 1991). A detailed interpretation of CSDs found for Mt. Etna lavas ought to take into account a law describing ΔT of each phase as a function of time and should include a suitable choice of the parameters adopted in Eqs. (6) and (7). This is far from our actual knowledge but is the direction of future research work.

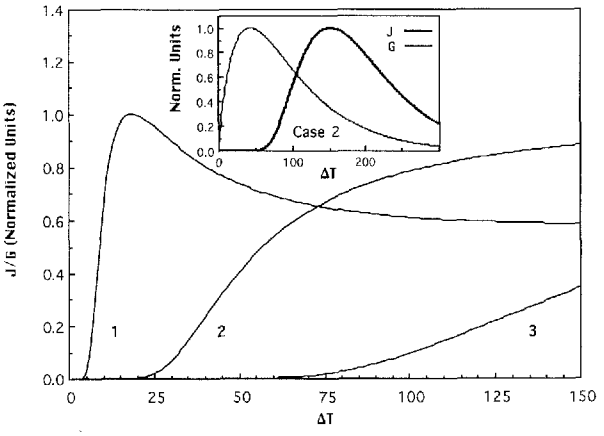

Fig. 10. Variation of the ratio J/G with undercooling. In the three reported cases $E = 200$ kJ/mol, $\Delta H = 60$ kJ/mol, while in Case 1: $\gamma = 0.02$ J/m^2, in Case 2: $\gamma = 0.05$ J/m^2 and in Case 3: $\gamma = 0.1$ J/m^2. Variations of E in the range $100 \div 200$ kJ/mol and of ΔH in the range $60 \div 80$ kJ/mol do not affect sensitively the curve. It is evident the strong increase of J/G in the initial part of the curve: we associate this portion to the explosive crystallization observed in range B. In the inset the shapes of nucleation and growth rate curves is reported respect to undercooling. All the curves are normalized with respect to their maximum value

Mixing phenomena in magma chambers have been suggested as a possible cause for the log linear dependence of $n(L)$ on crystal sizes (Marsh 1988). In these cases the slopes of CSDs are linked to a characteristic time τ during which the whole volume of a periodically filled (free of crystals) and periodically tapped magma chamber

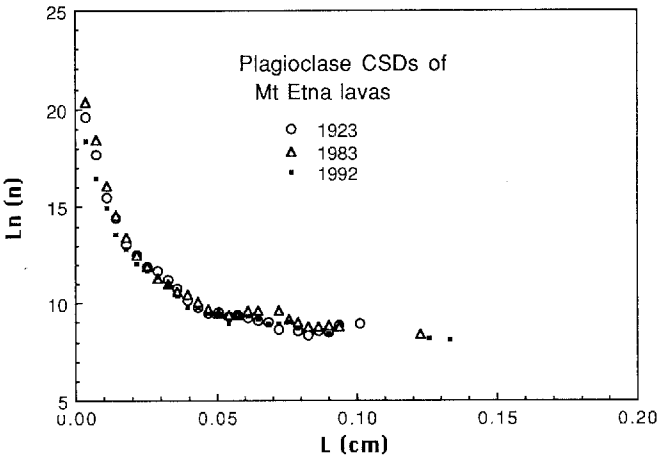

Fig. 11. CSDs of plagioclase for three different lavas of Mt. Etna. The pattern of CSD does not vary in spite of change in the output rate occurred in the meantime. Data collected at 16 × magnification

is completely renewed. Such systems may also experience changes in the refilling or output rates (i.e. variations in τ), that may cause kinks in CSDs. Output rates at Mt. Etna increased since the early 1970s, when the mean output rate of 0.2 m^3/s typical of the preceding two hundred years (Hughes et al. 1990) passed to 0.8 m^3/s (Armienti et al. 1989). Figure 11 shows plagioclase CSDs of lavas erupted in 1923, 1983 and 1989 with no evidence of change in the distributions, since kinks occur at the same values. This observation, when considered with the geochemical evidence, allows us to exclude that CSDs of Etnean lavas are due to mixing of different populations and strongly suggests that the main features of this system do not change in spite of observed variations in output rates.

Conclusions

Measurements of crystal size distributions for different minerals – olivine, plagioclase, clinopyroxene and oxides – of the 1991/93 Mt. Etna eruption display typical ranges related to magma cooling history. A nearly horizontal trend (range A) of CSDs in olivine, plagioclase and clinopyroxene populations suggests storage of the magma in a deep reservoir. Furthermore, the CSD of range A allows evaluation of crystal growth and nucleation rates at low undercooling, a condition difficult to maintain for sufficiently long time in experimental runs.

An increase in nucleation, revealed by CSD, could be related to magma ascent, when undercooling shows an increase. For plagioclase crystals belonging to the lower portion of range B (0.015 cm $< L <$ 0.05 cm), the habits reveal that the total undercooling was probably not more than 30°C; plagioclase crystals of the higher portion of B (0.003 cm $< L <$ 0.015 cm) reveal greater undercoolings.

Geophysical and geochemical evidence reveal that distinct pulses of magmas, each bearing similar CSDs, fed the volcano during the last two centuries. Lavas belonging to periods that fall astride major variations in the volcano output rate do not show changes in CSDs; this further supports the argument that Etna's plumbing system is basically different from that of other basaltic central volcanoes like Hawaii (Cashman and Marsh 1988; Mangan 1990) where the linear shape of CSDs is probably controlled by a reservoir continuously fed by crystal-free magma and periodically tapped by eruptions. In our case we ascribe the major variations in the number density of crystals in range B to depressurization-degassing effects ($H_2O + CO_2$) during magma ascent. Similar explosions of nucleation rates occur in other water-rich systems and have been related to the effects of gas release on the undercooling of magmas (Lipman et al. 1985; Cashman 1988, 1992). These observations lead to the far-reaching conclusion that, if the variations in undercooling responsible of crystal nucleation and growth are linked to degassing events, the effects of gas exsolution have not changed at Mt. Etna in the last two hundred years.

Appendix I

The errors introduced by the unfolding technique (Pareschi et al. 1990), numerically evaluated by a computer program, have been estimated by comparing some actual (hypothesized) crystal distributions in space and those reconstructed by the adopted unfolding technique. The grains are supposed to have a log linear distribution in space:

$$n(L) = n_o e^{-sL} \tag{1.1}$$

where n_0 and s are two given parameters. According to distribution (1.1) the total number of grains per unit volume is:

$$N_T = \int_0^\infty n(L)\, dL = \frac{n_o}{s} \tag{1.2}$$

and the probability density $\omega(L)$ is:

$$\omega(L) = \frac{n(L)}{\frac{n_o}{s}} = s\, e^{sL} \tag{1.3}$$

The probability of having a grain dimension occurring in the interval 0-L is:

$$\Omega(L) = \int_0^L \omega(L)\, dL = 1 - e^{-sL} \tag{1.4}$$

from which:

$$L = -\frac{1}{s} \ln(1-\Omega) \tag{1.5}$$

To verify the unfolding technique, that is the errors introduced by the algorithm on n_0 and s, the following steps have been performed (in the following, random numbers with uniform distribution between 0 and 1 have been generated by an algorithm by Calzolari 1976):

1. n_0/s uniform random numbers Ω_i ($i = 1,...,n_0/s$) have been generated between 0 and 1
2. For each of these numbers, a grain has been introduced with dimension L computed according to (1.5)
3. For each grain a random (with uniform distribution) distance d_L (between −0.5 and 0.5) from a reference plane $z = 0$ and a random (uniform) orientation θ_L (between 0 and $\pi/2$) have been generated, so that each grain is characterized by a triplet of numbers (L,d_L, θ_L)
4. For the grains intersecting the reference plane, the area of intersection has been evaluated; some tests have been performed in which we dropped the grains whose intersection area is lower than a minimum value, to simulate the effect of camera detection limit

Table 4. Assigned (columns 3 and 4) and reconstructed (columns 5 and 6) CSDs for spherical (C1÷C5) and elliptical (E1÷E6) particles

Case	e	Assigned		Calculated		Errors	
		$Ln(n_o)$	Slope s (cm^{-1})	$Ln(n_o)$	Slope s (cm^{-1})	$\Delta ln(n_o)/Ln(n_o)$	$\Delta s/s$
C1	0	15	100	14.3	102	4.7%	−2.0%
C2	0	15	200	15.7	234	−4.7%	−17.0%
C3	0	15	300	15.0	327	0.0%	−9.0%
C4	0	20	100	17.5	107	12.5%	−7.0%
C5	0	20	400	20.1	475	−0.5%	−18.7%
E1	0.2	15	150	15.3	173	−2.0%	−15.3%
E2	0.2	20	600	19.9	594	0.5%	1.0%
E3	0.3	20	200	17.9	186	10.5%	7.0%
E4	0.3	20	800	20.1	762	−0.5%	4.7%
E5	0.5	20	300	18.0	294	10.0%	2.0%
E6	0.5	20	1200	20.7	1076	−3.5%	10.3%

n_o is in cm^{-4}. Parameters n_o and s refer to crystals expected to have a log linear distribution $n(L)=n_o\exp(-sL)$. Column 2 reports particle elongation $e=(kL-L)/(kL+L)$. For spherical grains: $k=1$, $e=0$

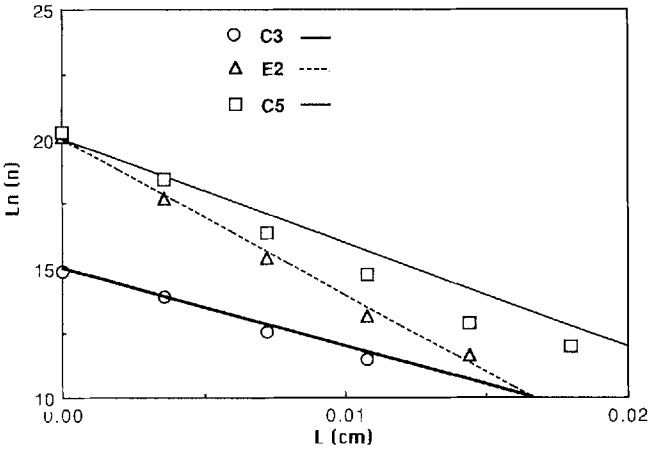

Fig. 12. Comparison between log linear assigned (lines) and reconstructed (symbols) CSDs in the case of spherical (C3 and C5) and elliptical (E2, see Table 4) particles, randomly distributed in the space. Symbols are the values obtained after the application of the unfolding procedure adopted for the computation of CSDs of Etnean lavas

5. The unfolding technique has been applied to the distribution of areas in the plane to reconstruct $n(L)$ in space, and the reconstructed data have been fitted by a straight line

Table 4 reports some assigned and unfolded CSDs with the relative values of $Ln(n_o)$ and s. The volume investigated was 1 cm^3 and the area considered for the unfolding process 1 cm^2. Both spherical particles (diameter L) and ellipsoidal grains (with axis kL,L,L and $k>1$) have been considered. For these, eccentricity e is defined as $(kL-L)/(kL+L)$, so that for spherical particles $e=0$. Figure 12 reports $n(L)$ as function of L in three cases (see Table 4) as assigned and reconstructed by the unfolding technique applied to spherical and elliptical grains; in Fig. 12 L of elongated particles refers to the minor axis of inertia. This implies that in Figs. 3–6 in text, where CSDs of plagioclase and clinopyroxene are respectively reported, the plotted linear dimensions have to be considered as the minor axes since these minerals have elongated shapes. Errors, resulting from Table 4, are, at maximum, in the order of 10%.

Some cases have been considered with the condition $k<1$ thus simulating tabular plagioclases. $Ln(n_o)$ is reconstructed with errors always below 5%, while reconstructed slopes are systematically higher. For example for $k=0.33$, $s=300$ and $Ln(n_o)=20$ the reconstructed value of s is 416 and $Ln(n_o)=19.8$ while for $k=0.25$, $s=300$ and $Ln(n_o)=20$ the reconstructed value of s is 571 and $Ln(n_o)=19.9$. A detailed treatment of the stereology of lenticular shapes indubitably deserves a more thorough treatment that is beyond the purposes of this study. It will be undertaken when using CSDs to work out a quantitative treatment of crystal growth in natural systems. In the assumed semi-quantitative approach the results of test cases guarantee that the obtained variations of CSD slopes are not artefacts introduced by the unfolding technique.

Tests, in which the occurrence of a size detection limit has been simulated, do not reveal any difference with CSDs reconstructed without considering this effect.

Appendix II

The area to be investigated in order to detect at least one crystal cut along its largest section (the particle is assumed to be a sphere of diameter L) can be computed according the formula:

$$\text{Area} = \frac{1}{2n(L)\,\Delta 1\,\sqrt{L\,\Delta 1}} \tag{2.1}$$

where Δl is the class size interval and $n(L)\,\Delta l$ is the number of crystals, per unit volume, with dimensions between $L-\Delta 1/2$ and $L+\Delta 1/2$). For population densities $n(L)<\exp(8)$ cm^{-4} (characteristic of millimetric crystals) the area to be investigated must be greater than 5 cm^2 (if $\Delta l = 0.002$ cm and $L \approx 0.1$ cm) and has to be 100 cm^2 for a density of exp(5) cm^{-4}. These areas become still larger if particles are elongated.

Appendix III

The crystal balance equation is (if crystal growth rate G is independent on crystal dimensions):

$$\frac{\partial \mathrm{Vn}}{\partial \mathrm{t}} + G\,\frac{\partial \mathrm{Vn}}{\partial \mathrm{L}} = 0 \tag{3.1}$$

with the initial and boundary conditions (letting $f(L,t) = n(L,t)V(t)$):

$$\mathrm{f}(L,t_i) = \begin{cases} 0 & \text{if } L > L_c \\ \dfrac{\mathrm{V}(t_i)\,J(t_i)}{G(t_i)} & \text{if } L = L_c \end{cases} \tag{3.2}$$

$$\mathrm{f}(L_c,t) = \frac{V(t)\,J(t)}{G(t)}$$

where t_i is the initial time and L_c the critical radius. These conditions come from the following considerations. The number of crystals in volume $V(t)$ with dimensions in the interval $L_c \div L_c + dL$ is $n(L_c,t)\ V(t)\ dL$, which is also equal to $J(t)\ V(t)\ dt$. Then:

$$n(L_c,t)\ V(t) = \frac{V(t)\ J(t)}{\frac{dL}{dt}} = \frac{V(t)\ J(t)}{G(t)} \tag{3.3}$$

since, for definition, $dL/dt = G$.

Along the characteristic curve $dL(t)/dt = G(t)$ (John 1971),which integrated gives:

$$L(t) = L_c + \int_{t_L}^{t} G(t)\ dt \tag{3.4}$$

the balance Eq. (3.1) can be rewritten as:

$$\frac{\partial f(L(t),t)}{\partial t} + \frac{dL(t)}{dt}\frac{\partial f(L(t),t)}{\partial L} = 0 \tag{3.5}$$

i.e.:

$$\frac{df(L(t),t)}{dt} = 0 \tag{3.6}$$

From (3.6) it follows that, along curve (3.4):

$$f(L(t),t) = \text{const.} = f(L_c,t_L) \tag{3.7}$$

where, according to (3.4), t_L is the time required by crystals of dimension L at time t, to grow from L_c to $L(t)$. But, according to boundary conditions (3.2):

$$f(L_c,t_L) = \frac{V(t_L)\ J(t_L)}{G(t_L)} \tag{3.8}$$

from which:

$$n(L,t) = \frac{V(t_L)\ J(t_L)}{G(t_L)\ V(t)} \tag{3.9}$$

Acknowledgement. We wish to thank K. Cashman and R.S.J Sparks for the suggestions that allowed us to improve an earlier version of the paper. During his sojourn in Pisa Dave Westerman shortened and polished the english version of the manuscript: we are grateful for his help in "limae labor". The present work has been carried out under the financial support of CNR - GNV. contract No. 91.02235.PF62.

References

Allard B, Sotin C (1988) Determination of mineral phase percentages in granular rocks by image analysis on a microcomputer. Comp Geosci 14:261–269

Armienti P, Clocchiatti R, D'Orazio M, Innocenti F, Petrini R, Pompilio M, Tonarini S, Villari L (1993) The long-standing 1991–1993 Mount Etna eruption: petrography and Geochemistry of lavas. Volcanol Acta (in press)

Armienti P, Innocenti F, Pareschi MT, Pompilio M, Rocchi S (1991) Crystal population density in not stationary volcanic systems: estimate of olivine growth rate in basalts of Lanzarote (Canary Islands). Mineral Petrol 44:181–196

Armienti P, Calvari S, Innocenti F, Pompilio M,Villari L (1990) Petrography and chemical composition. In: Barberi F, Bertagnini A, Landi P (eds) Mount Etna: the 1989 eruption. Giardini Pisa, pp 30–33

Armienti P, Innocenti F, Petrini R, Pompilio M, Villari L (1989) Petrology and Sr-Nd isotope geochemistry of recent lavas from Mt. Etna: bearing on the volcano feeding system. J Volcanol Geotherm Res 39:315–327

Armienti P, Calvari S, Innocenti F, Pompilio M,Villari L (1988) Sub-aphyric alkali basalts from Mt. Etna: inferences on the depth and composition of the source of magma. Rend Soc It Mineral Petrol 43:877–991

Barberi F, Carapezza ML, Valenza M, Villari L (1992) L'eruzione 1991–1992 dell'Etna e gli interventi per fermare o ritardare l'avanzata della lava. Giardini Pisa

Brandeis G, Jaupart C (1987) The kinetics of nucleation and crystal growth and scaling laws for magmatic crystallization. Contrib Mineral Petrol 96:24–34

Calzolari G, Cipriani TA, Corsi P (1976) Generation and testing of pseudo-random numbers with assigned statistical properties to be used in the stochastic simulation of econometric models. IBM Tech Rep n G513–3545

Cashman KV (1988) Crystallization of Mount St. Helens 1980–1986 dacite: a quantitative textural approach. Bull Volcanol 50:194–209

Cashman KV (1990) Textural constraints on the kinetics of crystallization of igneous rocks. Rev Mineral 24:259–314

Cashman KV (1992) Groundmass crystallization of Mount St. Helens dacite, 1980–1986: a tool for interpreting shallow magmatic processes. Contrib Mineral Petrol 109:431–449

Cashman KV, Marsh BM (1988) Crystal size distribution (CSD) in rocks and the kinetics and dynamics of crystallization. II: Makaopuhi lava lake. Contib Mineral Petrol 99:292–305

Clocchiatti R, Metrich N (1984) Témoignages de la contamination dans les produits des éruptions explosives des Mt. Silvestri (1892) et Mt. Rossi (1669). Bull Volcanol 47:909–928

Cooper RF, Kohlstedt DL (1982) Interfacial energies in the olivine-basalt system. In: Akimoto S, Manghnami MH (eds) High pressure research in geophysics, Adv Earth Plant Sci, vol 12, Center for Acadmic Publications Tokyo, pp 217–228

Cox KV, Bell J D, Pankhrust RJ (1979) The interpretation of igneous rocks. London, Allen and Unwin

Cristofolini R, Gresta S, Imposa S, Menza S, Patanè G (1987) An approach to problems of energy sources at Mount Etna based on seismological and volcanological data. Bull Volcanol 49:729–736

Dolfi D, Trigila R (1983) Clinopyroxene solid solutions and water in magmas: results in the system phonolitic tephrite-H_2O. Mineral Mag 47:347–351

Donaldson CH (1976) An experimental investigation of olivine morphology. Contrib Mineral Petrol 57:187–213

Dowty E (1980) Crystal growth and nucleation theory and numerical simulation of igneous crystallization. In: Hargraves RB (ed) Physics of magmatic processes. Princeton University Press, Princeton, pp 385–417

Ferrucci F (1990) Seismicity. In: Barberi F, Bertagnini A, Landi P (eds) Mount Etna: The 1989 eruption. Giardini, Pisa, pp 36–43

Ferrucci F, Rasà R, Gaudiosi G, Azzaro R, Imposa S (1993) Mt. Etna a model for the 1989 eruption. J Volcanol Geotherm Res 56:67–79

Ghiorso MS, Carmichael ISE., Rivers ML, Sack RO (1983) The Gibbs free energy of mixing of natural silicatic liquids: an expanded regular solution approximation for the calculation of magmatic intensive variables. Contrib Mineral Petrol 84:107–145

Hirn A, Nercessian A, Sapin M, Ferrucci F, Wittlinger G (1991) Seismic heterogeneity of Mt Etna: structure and activity. Geophys J Int 105:139–153

Hofmann AW (1980) Diffusion in silicate melts: a critical review. In: Hargraves RB (ed) Physics of magmatic processes. Princeton University Press, Princeton, pp 419–485

Hughes JW, Guest JE, Duncan AM (1990) Changing styles of effusive eruption on Mount Etna since AD 1600. In: Ryan MP (ed) Magma transport and storage. Wiley, pp 385–406

Jambon A, Lussiez P, Clocchiatti R, Weisz J, Hernandez J (1992) Olivine growth rate in a tholeiitic basalt: an experimental study of melt inclusions in plagioclase. Chem Geol 96:277–287

John F (1971) Partial differential equation. Springer, New York Berlin Heidelberg

Kilburn C (1989) Surface of aa flow-fields on Mount Etna, Sicily: morphology, rheology, crystallization and scaling phenomena. In: Fink J (ed) Lava Flows and Domes. Springer, Berlin Heidelberg New York, pp 129–156

Kirkpatrick RJ (1977) Nucleation and growth of plagioclase, Makaopuhi and Alae lava lakes, Kilauea Volcano, Hawaii. Geol Soc Am Bull 88:78–84

Kirkpatrick RJ, Gilpin RR, Hays JF (1976) Kinetics of crystal growth from silicate melts: anorthite and diopside. J Geophys Res 81:5715–5720

Lipman PW, Banks NG, Rhodes JM (1985) Degassing induced effects on lava rheology. Nature 317:604–607

Lofgren GE (1974) An experimental study of plagioclase crystal morphology: isothermal crystallization. Am J Sci 274:243–273

Lofgren GE (1980) Experimental studies on the dynamic crystallization of silicate melts. In: Hargraves RB (ed) The physics of magmatic processs. Princeton University Press, Princeton, pp 487–551

Maaløe S, Tumyr O, James D (1989) Population density and zoning of olivine phenocrysts in tholeiites from Kauai, Hawaii. Contrib Mineral Petrol 101:176–186

Macpherson GJ (1984) A model for predicting the volumes of vesicles in submarine basalts. J Geol 92:73–82

Mangan MT (1990) Crystal size distribution systematics and the determination of magma storage times: the 1959 eruption of Kilauea volcano, Hawaii. J Volcanol Geotherm Res 44:295–302

Marsh BD (1988) Crystal size distribution (CSD) in rocks and the kinetics and dynamics of crystallisation. I.Theory. Contrib Mineral Petrol 99:277–291

Metrich N, Clocchiatti R, Mosbah M (1993) The 1989–90 activity of Etna. Magma mingling and ascent of an H_2O-Cl-S rich basaltic magma. Evidence for the phenocryst melt inclusions. J Volcanol Geotherm Res (in press)

Montalto A, Distefano G, Patanè G (1992) Seismic patterns and fluid-dynamic features preceding and accompanying the January 15, 1990 eruptive paroxysm on Mt. Etna (Italy). J Vocanol Geotherm Res 51:133–143

Muncill GE, Lasaga AC (1987) Crystal-growth kinetics of plagioclase in igneous systems: one atmosphere experiments and approximation of a simplified growth model. Am Mineral 72:299–311

Pareschi MT, Pompilio M, Innocenti F (1990) Automated evaluation of volumetric grain-size distribution density from thin-section images. Comp Geosci 16:1067–1084

Scick R, Cosentino M, Lombardo G, Patanè G (1982) Volcanic tremor at Mt. Etna – a brief description. Mem Soc Geol It 23:191–196

Sobolev AV, Kamenetskiy VS, Metrich N, Clocchiatti R, Konokova NN, Devirts AL, Ustinov VI (1990) Volatile regime and crystallization conditions in Etna Hawaiite lavas. Geochymiya 9:1277–1290. (English translation)

Spohn T, Hort M, Fischer H (1988) Numerical simulation of the crystallization of multicomponent melts in thin dikes or sills. 1. The liquidus phase. J Geophys Res 93 B5:4880–4894

Toramaru A (1991) Model of nucleation and growth of crystals in cooling magmas. Contrib Mineral Petrol 108:106–117

Trigila R, Spera FJ, Aurisicchio C (1990) The 1983 Mount Etna eruption: thermochemical and dynamical inferences. Contrib Mineral Petrol 104:594–608

Weill DF, Hon R, Navrotsky A (1980) The igneous system $CaMgSi_2O_6$-$CaAl_2Si_2O_8$-$NaAlSi_3O_8$: variations on a classic theme by Bowen. In: Hargraves RB (ed) Physics of magmatic processes. Princeton University Press, Princeton, pp 49–92

Editorial responsibility: J. Hoefs